Metastable phase formation in the immiscible Cu–Co system studied by thermodynamic, molecular dynamics and *ab initio* calculations together with ion beam mixing

2007 J. Phys.: Condens. Matter 19 026219

(http://iopscience.iop.org/0953-8984/19/2/026219)

INSTITUTE OF PHYSICS PUBLISHING JOURNAL OF PHYSICS: CONDENSED MATTER

J. Phys.: Condens. Matter **19** (2007) 026219 (16pp) doi:10.1088/0953-8984/19/2/026219

Metastable phase formation in the immiscible Cu–Co system studied by thermodynamic, molecular dynamics and *ab initio* calculations together with ion beam mixing

H F Yan, Y X Shen, H B Guo and B X Liu[1]

Advanced Materials Laboratory, Department of Materials Science and Engineering, Tsinghua University, Beijing 100084, People's Republic of China

E-mail: dmslbx@tsinghua.edu.cn

Received 11 July 2006
Published 15 December 2006
Online at stacks.iop.org/JPhysCM/19/026219

Abstract

For the equilibrium immiscible Cu–Co system with a positive heat of formation of $+10$ kJ mol^{-1}, *ab initio* calculations were used to predict the physical properties of the metastable $D0_{19}$ and $L1_2$ structures for the $Cu_{75}Co_{25}$ phases and the $D0_{19}$ structure for the $Cu_{25}Co_{75}$ alloy. Based on the *ab initio* calculation results, an *n*-body Cu–Co potential was constructed and proven to be realistic. Applying the constructed Cu–Co potential, molecular dynamics simulations predict that the amorphous phase could be obtained at around $Cu_{60}Co_{40}$ and its atomic distribution could be inhomogeneous. Experimentally, by using ion beam mixing with 200 keV Xe^+ ions, an amorphous $Cu_{60}Co_{40}$ phase with inhomogeneous morphology was indeed obtained at a dose of 1×10^{15} Xe^+ cm^{-2}. Increasing the irradiation dose to 4×10^{15} Xe^+ cm^{-2}, a mixture of Cu-rich and Co-rich metastable phases was obtained. Besides, a mixture of FCC and HCP structures was observed in the $Cu_{82}Co_{18}$ multilayered sample and an HCP structure was observed in the $Cu_{26}Co_{74}$ multilayered sample. It was found that the lattice constants of the FCC and HCP phases determined by diffraction analysis were quite compatible with those predicted by the *ab initio* calculations.

1. Introduction

During the past decades, much attention has been paid to the formation of the metastable phases (including the amorphous phases) in the binary metal systems. Among the various

[1] Author to whom any correspondence should be addressed.

experimental methods, such as mechanical alloying [1–3], ion beam mixing [4, 5], vapour deposition [6, 7], pulse laser deposition [8] and vapour quenching [9], ion beam mixing (IBM) of multiplied metal layers has been proved to be one of the most powerful means for synthesizing metastable alloys in the binary metal systems [10]. With an effective cooling speed of 10^{13}–10^{14} K s^{-1} (estimated according to the so called thermal spike model) [11], IBM has successfully been employed in producing various metastable phases even in immiscible systems at equilibrium; e.g., in the Ag–W system with the largest positive heat of formation of +65 kJ mol^{-1}, amorphous alloys could be obtained by IBM [12, 13]. For the predictions of the metastable phases, theoretical models have also been greatly developed in recent years. Thermodynamically, Mediema's theory together with Alonso's method [12, 14, 15] is known to be a semi-empirical approach for predicting the possible non-equilibrium solid phases. At an atomic scale, molecular dynamics (MD) simulation is often regarded as a precise method in studying the interaction of the constituent atoms and the formation of metastable phases, as well as the structural phase transitions, of the binary metal systems [10, 16]. At an electronic scale, *ab initio* calculations (or first principles calculations) are also frequently employed to study the possible metastable phases in the binary metal systems; for example, Liu *et al* have applied the *ab initio* calculations in predicting some possible metastable phases of A_3B, AB_3 and AB types (A and B stand for the constituent metals of a system, respectively) [17, 18].

In the present study, we concentrated on studying the metastable phase formation in an equilibrium immiscible Cu–Co system through combining the theoretical modelling with the experimental confirmation by IBM. The Cu–Co system is characterized by a positive heat of formation of +10 kJ mol^{-1} [12]. Since the Cu atoms have similar atomic size to the Co atoms and the difference between the diffusivity of Co in Cu or vice versa and the self-diffusivity of Cu or Co is very small, it is considered that both the Cu atoms and the Co atoms could hardly intermix with each other in the equilibrium state. It had been reported that amorphization in the Cu–Co system was thermodynamically possible by far-from-equilibrium processing, yet was hard to achieve upon solid-state reaction (SSR) [19, 20]. Meanwhile, many significant phenomena like the precipitation behaviour [21, 22] and the phase separation [23, 24] in the Cu–Co alloys have been reported in the literature, yet the structural phase transition of the Cu–Co alloys has scarcely been studied. Consequently, the formation of metastable phases as well as the associated structural phase transition in the Cu–Co system is still far from understood and requires extensive studies both theoretically and experimentally.

In the present study, the thermodynamic calculation, *ab initio* calculation and MD simulations were employed to predict the possible metastable phases in the Cu–Co system. Experimentally, we used the IBM method to obtain confirmation of the theoretical predictions. Firstly, thermodynamic calculation based on Mediema's theory and Alonso's method was conducted to predict the possible metastable phases in the Cu–Co system, based on the calculated Gibbs free energy diagram of the system. Secondly, we identified/determined the structures, lattice constants, and cohesive energies of the possible metastable $Cu_{25}Co_{75}$, $Cu_{75}Co_{25}$ and $Cu_{50}Cu_{50}$ phases by conducting the *ab initio* calculations. Thirdly, under the framework of the second moment approximation of the tight-binding (TB-SMA) method [25, 26] we constructed an *n*-body Cu–Co potential through fitting the properties of those metastable Cu–Co alloy phases identified by *ab initio* calculation. Fourthly, applying the constructed *n*-body Cu–Co potential, we executed the MD simulations using the solid solution model to reveal the underlying physics of the structural phase transitions in the Cu–Co system. Finally, specially designed IBM experiments were carefully conducted to produce some Cu–Co metastable phases as well as to study the associated structural phase transitions, which were predicted by the above theoretical calculations.

2. Calculation methods and experimental procedure

2.1. Thermodynamic calculation

The Gibbs free energy of a non-equilibrium phase can be calculated by $\Delta G = \Delta H - T \cdot \Delta S$, where ΔH and ΔS are the enthalpy and entropy terms, respectively. As a first approximation based on Miedema's model [12, 14] and Alonso's method [15], the entropy term for a concentrated solid solution (CSS) and amorphous phase is simply taken as that of an ideal solution, i.e., $\Delta S = -R[C_A \ln C_A + C_B \ln C_B]$, where R is the gas constant and C_A and C_B are the atomic concentrations of metals A and B, respectively. The temperature T in the calculation is taken as 300 K.

The enthalpy change ΔH is the sum of three terms, i.e. $\Delta H_{MX} = \Delta H^c_{MX} + \Delta H^e_{MX} + \Delta H^s_{MX}$, corresponding to the chemical, elastic and structural contributions, respectively [12]. The chemical term ΔH^c_{MX} is accordingly calculated by $\Delta H^c_{MX} = \Delta H_{amp} V_A^{2/3} X_A f_{AB}$, where ΔH_{amp} is a constant amplitude for a specific system and can be obtained from the well documented literature [12]. The parameter f_{AB} is a function accounting for the degree to which atoms of type A are surrounded by atoms of type B, and is given by [27]

$$f_{AB} = X^S_B[1 + \gamma(X^S_A X^S_B)^2] \tag{1}$$

$$X^S_B = \frac{X_B V_B^{2/3}}{X_A V_A^{2/3} + X_B V_B^{2/3}}. \tag{2}$$

In equation (1), γ is an empirical constant describing the chemical short-range order (CSRO) of the solid solution, the amorphous and the ordered compounds, and is usually taken to be 0, 5 and 8, respectively.

For a non-equilibrium phase, the elastic energy is taken into account for the lattice distortion caused by atomic size mismatch of the two constituent metals. The elastic term is therefore expressed by

$$\Delta H^e_{MX} = X_A X_B[X_A \Delta H^e_{MX(B \text{ in } A)} + X_B \Delta H^e_{MX(A \text{ in } B)}], \tag{3}$$

where $\Delta H^e_{MX(i \text{ in } j)}$ is the elastic contribution to the heat of solution of constituent i in j in the non-equilibrium phase, and can be calculated by the method proposed by de Boer. For a non-equilibrium phase, the structural contribution to the free energy change is expressed by

$$\Delta H^s_{MX} = E(Z) - X_A E(Z_B) - X_B E(Z_A) \tag{4}$$

where $E(Z)$, $E(Z_A)$, $E(Z_B)$ are the lattice stabilities of the non-equilibrium phase and pure A and B metals, and Z, Z_A and Z_B are the average numbers of valence electrons of the non-equilibrium phase and the numbers of valence electrons of pure metals A and B, respectively. The dependence of the lattice stability on Z for paramagnetic and ferromagnetic transition metals has been calculated and can be found in the literature [28].

The Gibbs free energy of the initial state of the Cu–Co multilayered films should be calculated by adding the interfacial free energy to the ground state of a mixture of Cu and Co metals in the bulk form. Generally, the interfacial free energy is in positive proportion to the fraction of the interfacial atoms versus the total atoms in the films and can therefore be controlled by adjusting the number of the interfaces, while keeping the total thickness of the multilayered films constant [10]. In the present calculation, the total thickness of the Au–Co multilayered films is designed to be 40 nm and to consist of ten layers (namely five bilayers), in order to elevate the interfacial free energy of the Cu–Co multilayered films up to a highly energetic state, thus enabling us to obtain the corresponding non-equilibrium Cu–Co phase, which is in favour of the free energy concern.

2.2. Method of ab initio calculations

The Vienna *ab initio* simulation package (VASP) [29, 30] was used for the *ab initio* calculations to predict the possible metastable phases in the Cu–Co system. In VASP, the fully nonlocal ultrasoft Vanderbilt-type pseudopotentials [31] and the generalized-gradient approximation by Perdew and Wang [32] are applied to describe respectively the electron–ion interaction and the exchange and correlation items, allowing the use of a moderate cut-off for the construction of the plane-wave basis for the transition metals. The integration in the Brillouin zone is done on some special k points determined according to the Monkhorst–Pack scheme [33]. For the present calculation, the mesh of k points adopted is constitutive of 56 irreducible k points, which are sufficient for calculating the simple structures, and the cut-off energy for the plane-wave basis is 268.0 eV.

Generally, only some simple structures were selected for the *ab initio* calculations. (The detailed reason for the selection has been described in our recent publication [18].) Through the calculations over some simple structures, the relations of the cohesive energy per atomic volume versus the lattice constant for a selected metastable crystalline phase could be obtained. Comparing the calculated energies, it is therefore possible to predict the energetically favoured crystalline structures for the metastable phases at specific alloy compositions.

2.3. Methods in molecular dynamics simulations

2.3.1. Construction of an n-body Cu–Co potential. It is of vital importance for the performance of the MD simulations to have a realistic n-body potential. For the present Cu–Co system, an n-body Cu–Co potential was first constructed by the second-moment approximation of the tight-binding (TB-SMA) method [25, 26], which is suitable for dealing with both the hcp metal Co and the fcc metal Cu. In the TB-SMA, the total energy E_{total} of N atoms is written as

$$E_{\text{total}} = \sum_i \left\{ \sum_{j \neq i} A_{\alpha\beta} \exp\left[-p_{\alpha\beta} \left(\frac{r_{ij}}{r_{\alpha\beta}} - 1 \right) \right] - \sqrt{\sum_{j \neq i} \xi_{\alpha\beta}^2 \exp\left[-2q_{\alpha\beta} \left(\frac{r_{ij}}{r_{\alpha\beta}} - 1 \right) \right]} \right\} \quad (5)$$

where α and β denote respectively the two kinds of constituent atoms; r_{ij} is the distance between atom i and atom j; $d_{\alpha\beta}$ is the first-neighbour distance; A, p, ζ and q are four adjustable parameters. In construction of a realistic n-body potential, it is essential to fit the parameters for both the potentials of pure metals Co and Cu as well as the Cu–Co cross potential. In the present study, the potential parameters for the pure metals Co and Cu were fitted with the experimental data of some physical properties (i.e., the cohesive energy, the lattice constant, the bulk modulus, the elastic constants and the vacancy formation energy) of the two metals. Since there are no existing data for any equilibrium alloy in the Cu–Co system, the parameters of the Cu–Co cross potential were fitted with the physical properties of some metastable crystalline phases, which were identified/determined by *ab initio* calculations. In fitting, the cut-off distance is fixed to be 6.0 Å, which corresponds to the ninth nearest distance in both the hcp Co structure and the fcc Cu structure.

2.3.2. Simulation scheme, simulation models and characterization methods. We performed the molecular dynamics simulations with the Parrinello–Rahman constant pressure scheme, in which the equations of motion were solved through a second-order four-value predictor–corrector algorithm of Gear with a time step of $t = 5 \times 10^{-15}$ s [34]. All the simulation models were set to have the same number of atoms in the computational box, whose initial [100], [010] and [001] atomic crystal directions are parallel to the x, y and z axes, respectively. Since the periodic boundary conditions were adopted in all three dimensions, the computational

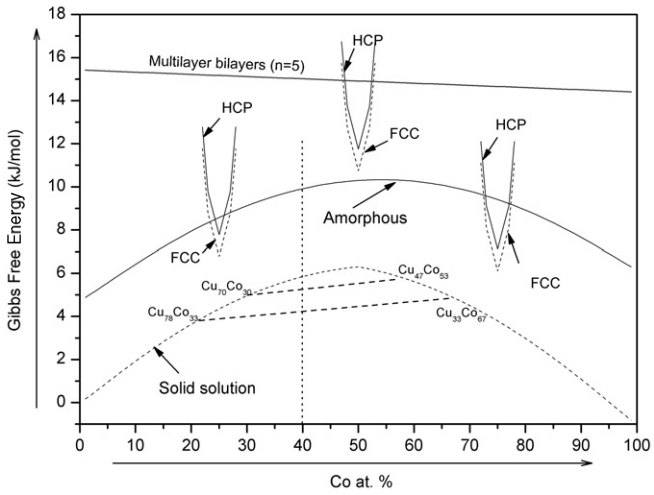

Figure 1. The calculated Gibbs free energy of the Cu–Co system based on Miedema's theory and Alonso's method.

box can be imagined to be replicated to infinity by rigid translation in all three Cartesian directions, virtually eliminating the surface effects of the system and the position effect of the box boundaries. In the present study, the computational box was set to be a system of $9 \times 9 \times 9$ fcc unit cells, with 2916 atoms. The initial fcc solid solution model was obtained by randomly substituting a certain number of Co atoms into the Cu fcc lattice and then run at 300 K for adequate MD time steps ($\sim$2 ns) to reach a relatively stable state, at which all the dynamic parameters showed no secular variation.

To trace the atomic movement, the most direct and convenient way was to inspect the projections of the atomic positions, presenting a visualized atomic picture of the structural phase transition revealed by the MD simulations. As the variation of the pair-correlation function $g(r)$ was commonly recognized as a decisive parameter to identify an amorphous structure, the $g(r)$ for a block of materials was also calculated in the present study to quantitatively monitor the process of the structural transition in the models [35].

2.4. Experimental procedure of ion beam mixing

2.4.1. Design and preparation of the Cu–Co multilayered films. We studied the metastable phase formation by irradiating some specially designed Cu–Co multilayered films with a 200 keV xenon ion beam. To match the projected range plus projected range straggling of the 200 keV xenon ions for an effective intermixing, the total thickness of the Cu–Co multilayered films was designed, according to the TRIM code [36], to be about 40 nm, and the design of the layer numbers and the thicknesses of the individual layers was based on the interfacial free energy calculation [10]. Since the Gibbs free energy curves of the multilayered films, the amorphous phase, the solid solution and the possible metastable HCP and FCC phases in figure 1 indicate that the Cu–Co multilayered films with ten layers (five bilayers) have high enough free energy, we prepared all the Cu–Co multilayered films with a total of ten layers and each individual layer was designed to be greater than 20 Å to ensure obtaining continuous deposited layers. Through alternately depositing pure metals Cu and Co onto NaCl single-crystal substrates, the designed Cu–Co multilayered films were prepared with a deposition

rate of 0.5 Å s^{-1} in an ultrahigh-vacuum (UHV) e-gun evaporation system at a vacuum level better than 3.0×10^{-6} Pa. After deposition, the real compositions of the as-deposited Cu–Co multilayered films were confirmed by the energy-dispersive spectrum (EDS) analysis to be $Cu_{26}Co_{74}$, $Cu_{60}Co_{40}$, $Cu_{82}Co_{18}$, respectively, with a measuring error around 5%.

The as-deposited films were then subjected to 200 keV xenon ion irradiation to doses ranging from 1×10^{15} to 7×10^{15} Xe^{+} cm^{-2}, in an implanter with a base vacuum level of 10^{-4} Pa. During the irradiation, the sample holders were cooled by liquid nitrogen (77 K) and the ion current density was controlled to be less than 1 μA cm^{-2} to avoid overheating. Under such precautions, the temperature of the Cu–Co multilayered films was estimated to be only a little higher than 77 K. For structural characterization, the Cu–Co multilayered films were removed from the NaCl substrates by de-ionized water and placed onto the Mo grids for the transmission electron microscopy (TEM) observation and selected area diffraction (SAD) analysis. The structures in the as-deposited states and those resultant Cu–Co phases upon 200 keV xenon IBM were identified from the respective SAD patterns. A high-resolution electron micrograph (HREM) was employed to obtain an intuitionistic image of the atomic distribution of the metastable phases formed by IBM. The lattice constants of the resultant Cu–Co crystalline phases were determined by the corresponding SAD patterns with an error of about 5%.

3. Results and discussion

3.1. Structures of some metastable Cu–Co phases predicted by ab initio calculations

Ab initio calculations were performed to predict the lattice constants and the cohesive energies of some metastable crystalline phases in the Cu–Co system. In the present study, the correlation between the total energy and the average atomic volume for the $D0_{19}$, $D0_3$, $D0_9$, $L1_2$, $L6_0$ and A15 structures of the $Cu_{75}Co_{25}$ and $Cu_{25}Co_{75}$ phases, and the B1, B2, B3, $L1_0$, α-NiAs and $L2_a$ structures of the $Cu_{50}Co_{50}$ phases were obtained and are shown in figures 2(a)–(c), respectively. From figures 2(a)–(c), the $D0_{19}$ and $L1_2$ $Cu_{75}Co_{25}$, the $D0_{19}$ $Cu_{25}Co_{75}$ and the $L1_0$ $Cu_{50}Co_{50}$ phases have the lowest energies among the calculated structures; i.e., these structures were predicted to be relatively stable among the possible ones.

The calculated results of the lattice constants (a and c/a), the atomic volumes (V) and the minimum cohesive energy ($E_{\min}$) are listed in table 1 for the above mentioned structures. The structures marked with asterisks have the lowest cohesive energies, corresponding to the most possible structures of the metastable $Cu_{75}Co_{25}$, $Cu_{25}Co_{75}$ and $Cu_{50}Co_{50}$ phases, respectively.

3.2. Metastable phases predicted by molecular dynamics simulations

3.2.1. Parameter fitting for a realistic n-body Cu–Co potential. The n-body potential for the Cu–Co system includes the potentials of the pure metals (i.e. of pure Co and pure Cu) and the Cu–Co cross potential. The potential parameters of the pure metals were fitted with the experimental data of the pure metals and the parameters for the Cu–Co cross potential were fitted with the lattice constants and the cohesive energies of the $L1_2$ $Cu_{75}Co_{25}$ phase and the B2 $Cu_{50}Co_{50}$ phase obtained by the *ab initio* calculations. The fitted parameters of the Cu–Co system are listed in table 2. For a verification of the constructed n-body potential, the cohesive energies, the lattice constants, the bulk modulus, the elastic constants and the vacancy formation energies for the pure metal Cu and metal Co could be reproduced by the constructed potential and the data are listed in table 3. Moreover, the lattice constants and the cohesive energies of the $D0_{19}Cu_{25}Co_{75}$ and $Cu_{75}Co_{25}$ phases, the $L1_2$ $Cu_{25}Co_{75}$ and $Cu_{75}Co_{25}$ phases

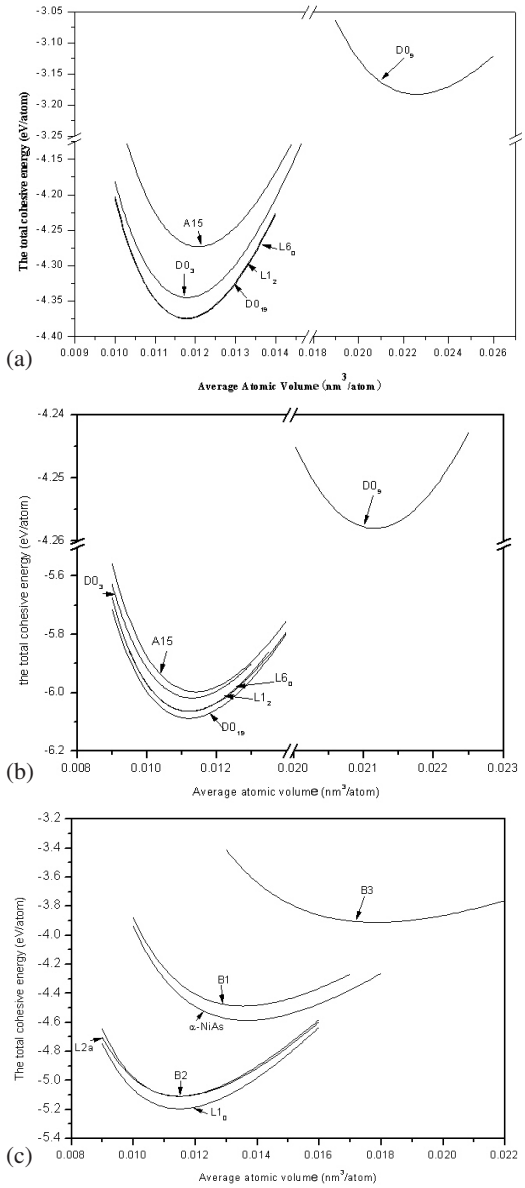

Figure 2. The calculated total energy versus the lattice constant for (a) $Cu_{75}Co_{25}$, (b) $Cu_{25}Co_{75}$ and (c) $Cu_{50}Co_{50}$ metastable phases of different structures by *ab initio* calculation.

and the B2 $Cu_{50}Co_{50}$ phase were calculated by the constructed potential and are listed in table 4. From table 4, one can see that the *ab initio* calculated values of the cohesive energies and the lattice constants for the above mentioned phases could also be reproduced by the constructed potential, confirming the relevance of the constructed Cu–Co potential.

3.2.2. Simulation results of the metastable Cu–Co phases. With the constructed *n*-body Cu–Co potential, MD simulations were executed at 300 K with three FCC solid solution models with overall compositions of $Cu_{25}Co_{75}$, $Cu_{60}Co_{40}$ and $Cu_{75}Co_{25}$, respectively.

Table 1. The calculated equilibrium cohesive properties (lattice constants a and c/a, atomic volume V, cohesive energy $E_{\min}$) of $Cu_{75}Co_{25}$, $Cu_{50}Co_{50}$ and $Cu_{25}Co_{75}$ structures from *ab initio* calculation. (Note: the values with asterisks (*) are for the structures with lowest cohesive energies.)

$Cu_{75}Co_{25}$	$D0_{19}$	$D0_3$	$D0_9$	$L1_2$	$L6_0$	A15
a (Å)	2.56	5.74	4.49	3.61	3.60	4.58
c/a	1.63				1.006	
V (Å^3/atom)	11.780	11.799	22.581	11.768	11.773	12.065
$E_{\min}$ (eV/atom)	−4.3753*	−4.3453	−3.1828	−4.3748*	−4.3745	−4.2734
$Cu_{50}Co_{50}$	B1	B2	B3	$L1_0$	$L2_a$	α-NiAs
a (Å)	4.77	2.84	5.23	3.50	2.92	3.62
c/a				1.07	0.92	1.33
V (Å^3/atom)	13.548	11.461	17.831	11.488	11.502	13.659
$E_{\min}$ (eV/atom)	−4.4871	−5.1084	−3.9114	−5.1946*	−5.1078	−4.5857
$Cu_{25}Co_{75}$	$D0_{19}$	$D0_3$	$D0_9$	$L1_2$	$L6_0$	A15
a (Å)	2.51	5.65	4.39	3.55	3.55	4.50
c/a	1.63				0.999	
V (Å^3/atom)	11.198	11.282	21.151	11.204	11.200	11.387
$E_{\min}$ (eV/atom)	−6.0875*	−6.0179	−4.2580	−6.0639	−6.0634	−5.9966

Table 2. The potential parameters for the Cu–Co system.

	A (eV)	ξ (eV)	p	q	r_0 (Å)	$r_{\text{cut-off}}$ (Å)
Co–Co	0.1140	1.5554	10.8835	2.3780	2.497	6.0
Cu–Cu	0.0963	1.2658	10.3542	2.4010	2.560	6.0
Co–Cu	0.0662	1.1047	10.8133	1.5417	2.5416	6.0

Table 3. Physical properties of fitted quantities and experimental quantities. The energies are in units of electron volts (eV), lattice constants in angstroms (Å) and elastic constants in 10^{11} Pa.

	a[a]	$-E_C$[b]	C_{11}	C_{12}	C_{44}	C_{13}	C_{33}	E_{vf}
Cu	3.62	3.52	1.7[c]	1.225[c]	0.758[c]			1.30[d]
			1.6948	1.228	0.7588			1.217
Co	2.50	4.39	3.071[c]	1.65[c]	0.755[c]	1.027[c]	3.581[c]	1.35[e]
			3.0815	1.4309	0.6243	1.2334	3.4532	1.5694

[a] Reference [39]; [b] Reference [40]; [c] Reference [41]; [d] Reference [42]; [e] Reference [43].

Table 4. Comparison between VASP calculations and potential derivatives. The lattice constants are in angstroms (Å) and cohesive energies in electron volts/atom (eV/atom).

	Ab initio calculation		Potential derivatives	
	A	E_c	a	E_c
$L1_2CuCo_3$	3.55	4.3003	3.63	4.2852
$D0_{19}CuCo_3$	5.02	4.2766	4.97	4.2807
B_2CoCu	2.84	4.2087	2.95	4.2212
$L1_2Cu_3Co$	3.61	3.8952	3.67	3.8487
$D0_{19}Cu_3Co$	5.11	3.8947	5.02	3.8571

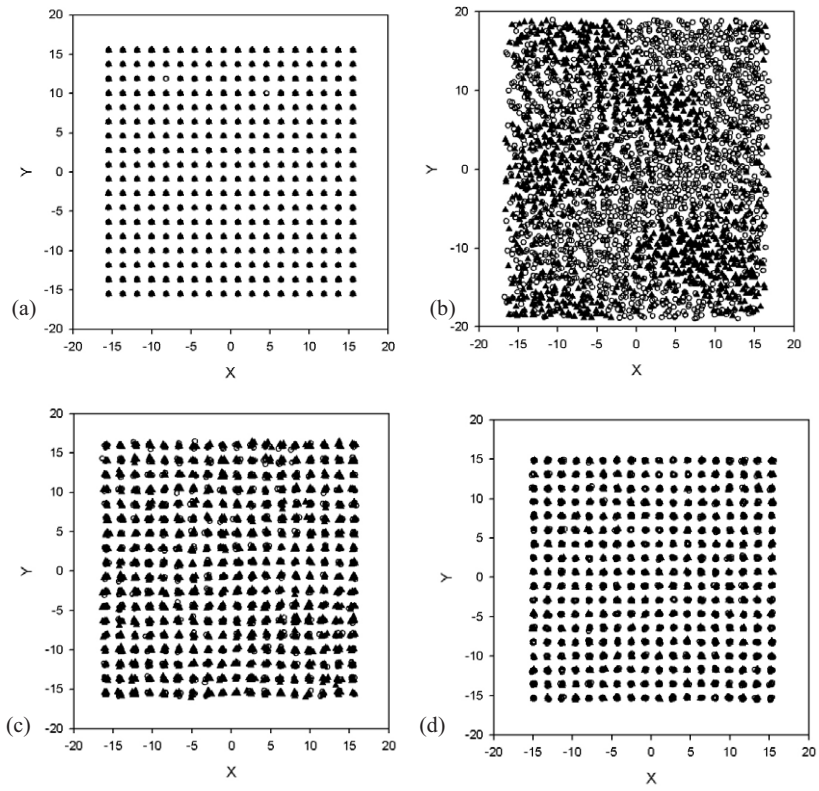

Figure 3. Projections of the atoms on the x–y plane: (a) the $Cu_{60}Co_{40}$ solid solution in the initial state; (b) the $Cu_{60}Co_{40}$, (c) the $Cu_{25}Co_{75}$ and (d) $Cu_{75}Co_{25}$ solid solutions after annealing at 300 K for 2 ns, respectively. Open circles and filled triangles stand for the Co atoms and Cu atoms, respectively.

After annealing for 2 ns, the $Cu_{60}Co_{40}$ solid solution model was found to have collapsed into a disordered state, while other two models kept their ordered crystalline lattice configurations. Figures 3(a) and (b) show the atomic position projections of the $Cu_{60}Co_{40}$ solid solution at initial state and the state after annealing for 2 ns at 300 K. From figure 3(b), one sees that the initial FCC structure has been turned into a disordered state, which can be confirmed to be an amorphous structure by the calculated total pair correlation function $g(r)$ shown in figure 4. One sees that the $g(r)$ curves in figure 4(b) become smoother and have less peak than those shown in figures 4(a) and (c), indicating that an amorphous phase is formed in the $Cu_{60}Co_{40}$ model. The disordered structure in figure 3(b) actually appears in a mixture of a Cu-rich part and a Co-rich part, and the two different parts spread and interconnect with each other in three dimensions randomly, forming an amorphous structure as a whole. Such a phenomenon has once been observed in the irradiation experiment [22] and confirmed by kinetic Monte Carlo (KMC) simulations [23]. Consequently, MD simulation is quite reliable to predict the amorphization behaviour in the immiscible Cu–Co system with a realistic n-body potential. Meanwhile, the other four solid solution models remain in crystalline structures even after annealing for more than 2 ns, e.g. as shown in figures 3(c) and (d), the atomic position projections of the $Cu_{25}Co_{75}$ and $Cu_{75}Co_{25}$ solid solutions, respectively. It is clear that both are FCC lattices even after annealing for 2 ns. From the pair correlation functions of the

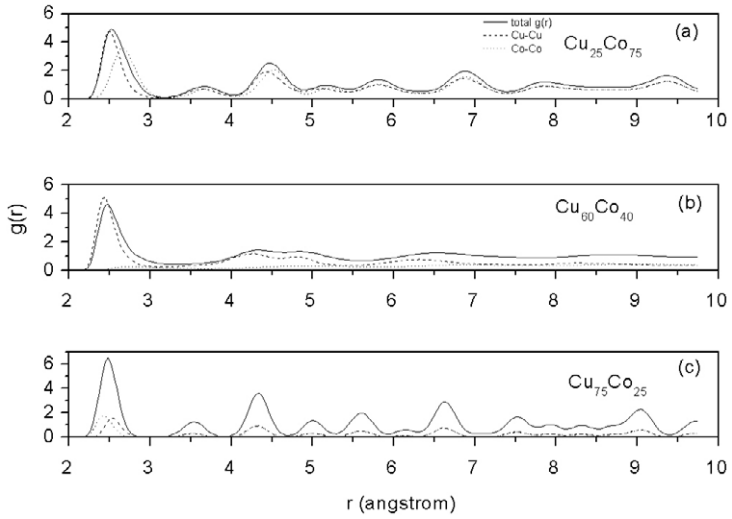

Figure 4. The calculated total pair correlation functions of the (a) $Cu_{25}Co_{75}$, (b) $Cu_{60}Co_{40}$ and (c) $Cu_{75}Co_{25}$ solid solutions, respectively, upon annealing at 300 K for 2 ns. The solid line is for the total $g(r)$, the short-dashed line is for the Cu–Cu partial $g(r)$ and the dotted line is for the Co–Co partial $g(r)$.

Table 5. Structural changes of Cu–Co multilayered films upon 200 keV xenon-ion-beam mixing at 77 K. 'Cu + Co' represents a mixture of crystalline Cu and Co; FCC-I and FCC-II present two different crystalline structures with different lattice constants; so do HCP-I and HCP-II.

Dosage (Xe^+ cm^{-2})	$Cu_{26}Co_{74}$	$Cu_{60}Co_{40}$	$Cu_{82}Co_{18}$
As-deposited	Cu + Co	Cu + Co	Cu + Co
1×10^{15}	HCP-II	Amorphous	FCC-I + HCP-I
4×10^{15}	HCP-II	FCC-I + FCC-II	FCC-I + HCP-I
7×10^{15}	HCP-II	FCC-I + HCP-II	FCC-I + HCP-I

$Cu_{75}Co_{25}$ and $Cu_{25}Co_{75}$ in figures 4(a) and (c), the lattice constants of $Cu_{25}Co_{75}$ and $Cu_{75}Co_{25}$ structures were determined to be 3.54 and 3.62 Å, respectively, which are quite compatible with those of the $L1_2$ $Cu_{75}Co_{25}$ and the $L1_2$ $Cu_{25}Co_{75}$ phases, respectively, predicted by *ab initio* calculations.

3.3. Metastable phases formed by ion beam mixing

Performing IBM with 200 keV xenon ion beams at 77 K, three multilayered samples (the $Cu_{60}Co_{40}$, the $Cu_{82}Co_{18}$ and the $Cu_{26}Co_{74}$) were investigated in the present study for the metastable phase formation in the Cu–Co system and the experimental results are listed in table 5.

In the $Cu_{82}Co_{18}$ multilayered sample, a mixture of an FCC structure ($a = 3.62$ Å) and an HCP structure ($a = 2.62$ Å and $c/a = 1.65$) (determined from the SAD patterns in figure 8(a)) was observed after a dose of 1×10^{15} Xe^+ cm^{-2}. With the same lattice constants and almost the same compositions, the observed FCC structure and the HCP structure were reasonably inferred to be respectively the $D0_{19}$ (HCP) and the $L1_2$ (FCC) structures of the $Cu_{75}Co_{25}$ phases predicted by *ab initio* calculation, and the structural phase transition process in the sample could

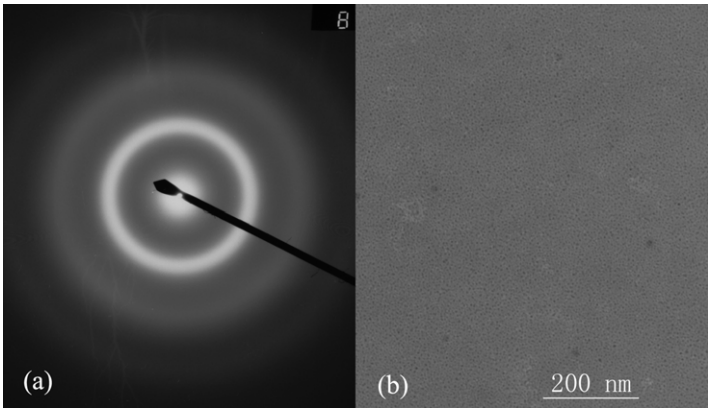

Figure 5. (a) The SAD pattern and (b) the bright-field image of the amorphous phase in the $Cu_{60}Co_{40}$ film.

be summarized as

$$Cu_{82}Co_{18} \xrightarrow{1\times10^{15}\ Xe^{+}\ cm^{-2}} \text{FCC } (a = 3.62\ \text{Å}) + \text{HCP } (a = 2.62\ \text{Å and } c/a = 1.65).$$

As for the $Cu_{26}Co_{74}$ multilayered sample, a uniform metastable HCP structure ($a = 2.55$ Å and $c/a = 1.65$) was obtained after irradiation to a dose of 1×10^{15} Xe^{+} cm^{-2} and its SAD pattern was shown in figure 8(b). Similarly, the HCP phase could be considered the same kind as the $D0_{19}$ $Cu_{25}Co_{75}$ phase predicted by *ab initio* calculation, and the structural phase transition process in the sample could be summarized as

$$Cu_{26}Co_{74} \xrightarrow{1\times10^{15}\ Xe^{+}\ cm^{-2}} \text{HCP } (a = 2.55\ \text{Å and } c/a = 1.65).$$

In the $Cu_{60}Co_{40}$ multilayered sample, an amorphous phase was observed after irradiation to a dose of 1×10^{15} Xe^{+} cm^{-2} and the whole morphology of the amorphous phase seemed to be inhomogeneous in the TEM bright-field image, which is similar to the results from MD simulations mentioned above. Figures 5(a) and (b) show the SAD pattern and the TEM bright-field image of the obtained amorphous phase, respectively. For an accurate determination of the atomic distribution, HREM was employed with a multiple of 5×10^{6} and the atomic distribution image of the obtained amorphous phase was found to be composed of two different areas, i.e. (a) the bright area and (b) the dark area, correspondingly shown in figure 6. Analysed with the Fourier fast transformation (FFT) [37], both areas were determined to be amorphous and the dark area contained more Cu atoms (measured by EDS) than the bright area, while the bright area contained more Co atoms than the dark area. Interestingly, in the $Cu_{60}Co_{40}$ multilayered sample, after irradiation to a dose of 4×10^{15} Xe^{+} cm^{-2}, a mixture of two FCC structures with different lattice constants was observed. Figures 7(a) and (b) show respectively the corresponding SAD pattern and the TEM bright-field image. From the SAD patterns, the lattice constants of the two FCC structures could be determined to be $a = 3.62$ and 3.52 Å, respectively. In addition, the dark areas in the TEM bright-field image stand for the areas with more Cu, while the bright area for more Co. Comparing with the above mentioned amorphous phase, the composition difference (determined by EDS) in both the dark and the bright areas has been increased. Further increasing the irradiation dose up to 7×10^{15} Xe^{+} cm^{-2}, the structures emerged in the $Cu_{60}Co_{40}$ multilayered sample changed into a mixture of an FCC structure ($a = 3.61$ Å) and an HCP structure ($a = 2.52$ Å, $c/a = 1.62$). The corresponding SAD pattern and the TEM image are shown respectively in figures 7(c) and (d). Comparing

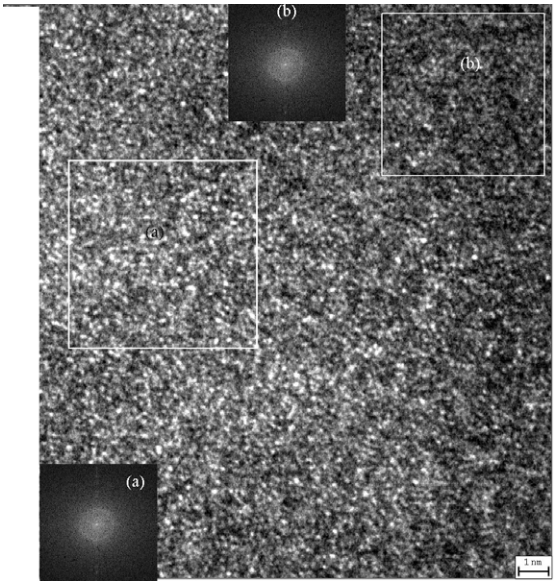

Figure 6. The HREM image and the FFT results (a) for the bright Co-rich area and (b) for the dark Cu-rich area, respectively, in the $Cu_{60}Co_{40}$ amorphous phase.

figure 7(d) with (b), both the dark and bright areas, as well as the composition difference in those two areas, are further increased. In summary, the structural phase transition along with the irradiation dose in the $Cu_{60}Co_{40}$ multilayered sample can be expressed by

$$\begin{aligned} \mathrm{Cu_{60}Co_{40}\ (multilayer)} &\xrightarrow{1\times10^{15}\ \mathrm{Xe^{+}\ cm^{-2}}} \text{amorphous} \\ &\xrightarrow{4\times10^{15}\ \mathrm{Xe^{+}\ cm^{-2}}} \text{FCC-I } (a = 3.62\ \text{Å}) + \text{FCC-II } (a = 3.52\ \text{Å}) \\ &\xrightarrow{7\times10^{15}\ \mathrm{Xe^{+}\ cm^{-2}}} \text{FCC-I } (a = 3.61\ \text{Å}) + \text{HCP } (a = 2.52\ \text{Å}, c/a = 1.62). \end{aligned}$$

In order to interpret the structural phase transition, it is of importance to briefly review the physical process of IBM, which is known to be divided into two consecutive steps, i.e. the first step of an atomic collision followed by a second step of relaxation. During the first step, the energy of the irradiating ions was 200 keV, while the binding energies of the metals Cu and Co are on the order of 5–10 eV, which is much smaller than that of the irradiating ions. Consequently, the irradiating ions would trigger a series of atomic collisions, namely an atomic collision cascade, which is responsible for inducing atomic mixing between the Cu and Co layers as well as for driving the resultant Cu–Co mixture into a far-from-equilibrium state, which is most likely in a disordered state. After irradiation to an adequate dose inducing enough atomic mixing, the discrete layered structure of the Cu–Co multilayered sample was smeared out and a uniform disordered Cu–Co mixture in a highly energetic state is obtained. At the moment of termination of the atomic collision cascade, the equilibrium thermodynamics comes into play, giving the direction for the disordered Cu–Co mixture to relax towards equilibrium. However, as the relaxation time period is extremely short, lasting only for 10^{-10}–10^{-9} s, the disordered Cu–Co mixture cannot undergo straightforward relaxation to an equilibrium state; instead, it frequently resides at one of the possible non-equilibrium/intermediate states, which could be amorphous and simple crystalline structured phases. For instance, in the present study, in some Cu–Co samples, after irradiation to an appropriate dose, uniform mixing was

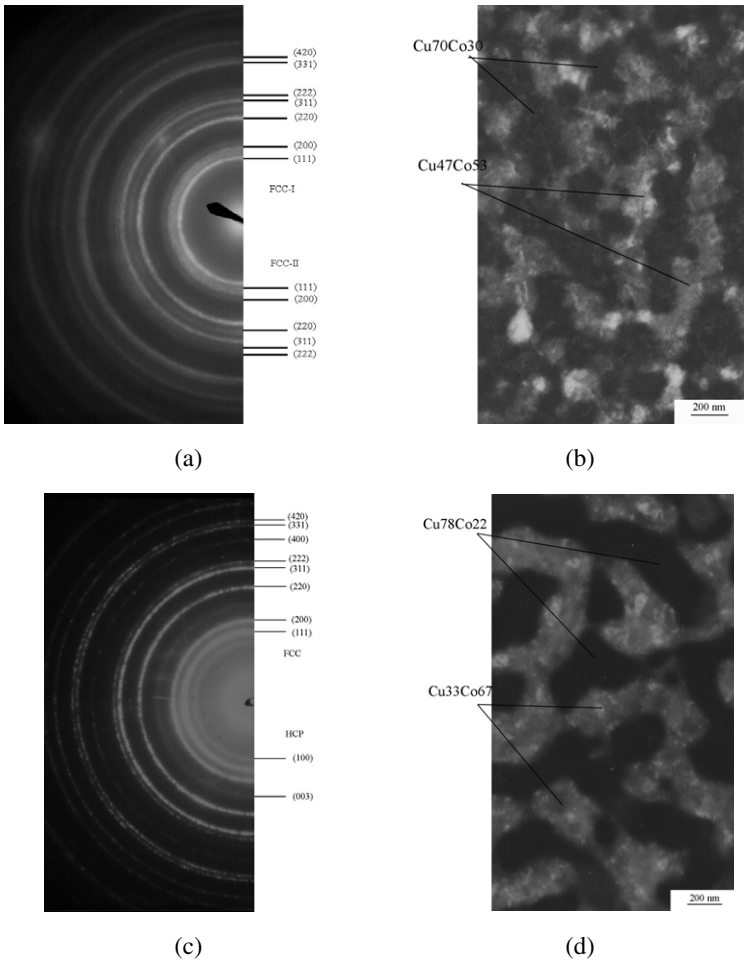

Figure 7. (a) The SAD pattern and (b) the bright-field image of the mixture of two FCC structures after the amorphous phase is irradiated at a dose of 4×10^{15} Xe^{+} cm^{-2}. (c) The SAD pattern and (d) the bright-field image of the mixture of FCC and HCP structures after the amorphous phase is irradiated at a dose of 7×10^{15} Xe^{+} cm^{-2}.

achieved, and during the very restricted time period of relaxation the disordered state remained, resulting in forming an amorphous phase. Actually, the higher the irradiation dose is, the more atomic motion is so induced, leading to the opportunity for the other competitive phases to appear, which, on the other hand, would frustrate the formation of the amorphous phase. It is therefore deduced that if one takes into account the competition between amorphization and other metastable phases upon IBM the composition region favouring metallic glass formation may be reduced and amorphization could thus be missed in experiments.

We now turn to discuss the metastable phase formation of the Cu–Co system by IBM, in terms of the calculated Gibbs free energy diagram of the system shown in figure 1. In the figure, obviously for the Cu–Co multilayered films consisting of five or more bilayers, the interfacial free energy was high enough to evaluate the initial energetic state of the films to a level higher than those of the metastable phases. Note that the free energy curves of the metastable hcp and fcc phases are schematically narrow because they are considered to be compound-like.

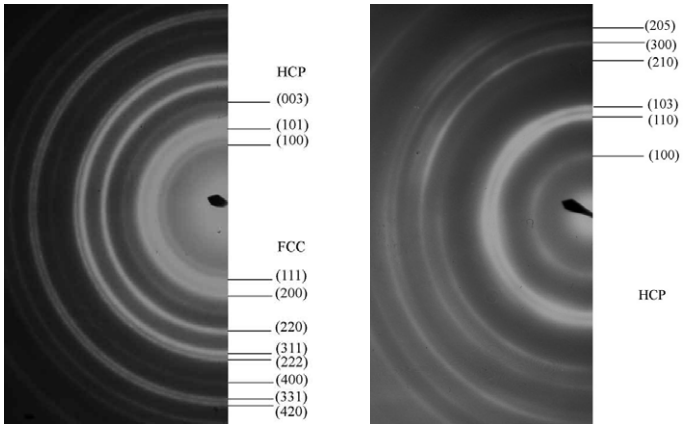

Figure 8. The SAD patterns of (a) the $Cu_{82}Co_{18}$ film and (b) the $Cu_{26}Co_{74}$ film.

Firstly, according to the Gibbs free energy diagram, the free energy curve of the Cu–Co amorphous phase was calculated to be higher than that of the Cu–Co solid solution and therefore is highly metastable. In IBM, after irradiation to an appropriate dose, a highly energetic disordered Cu–Co mixture could be obtained and its free energy is even higher that of the amorphous phase. Consequently, the Cu–Co amorphous phase could be formed from the highly energetic atomic mixture at an appropriate temperature and time condition available during the relaxation period. According to the well known Ostwald step rule [38], the $Cu_{60}Co_{40}$ amorphous phase could be firstly obtained, because it was the nearest metastable state to the initial state in terms of the free energy. In addition, it can be found in the Gibbs free energy diagram that more metastable phases including the compound-like phases and solid solutions with close Gibbs free energies would take part in the competition with the amorphous phase near the two terminals rather than in the middle of the composition range, where the amorphous phase is more favoured to be formed than the other metastable phases.

Secondly, the Cu–Co solid solutions were obtained upon high doses, mainly because the over-irradiated doses of IBM induced the composition fluctuation as well as the temperature in the amorphous phase and thus enhanced the possibility for the crystallization of other possible metastable Cu–Co phases in the system, when the dose went even higher than that required for a uniform mixing. Consequently, the crystallization of the possible Cu–Co crystalline phase was possibly obtained in the competition of any other metastable phases, resulting in a frustration of the amorphous phase, which was predicted to be unstable and inhomogeneous topologically by theoretical calculation.

Thirdly, because the solid solution lines were convex as usual in the positive ΔH_f systems, the phase separation in the Cu–Co solid solution was reasonable, i.e., the mixture of two solid solutions with different compositions was more favourable energetically than a single solid solution, which was also illustrated in the Gibbs free energy diagram.

4. Concluding remarks

(1) We have shown that *ab initio* calculations could be used to predict the physical properties of some metastable structures in the equilibrium immiscible Cu–Co system and that molecular dynamics simulations could be applied to investigate the structural phase

transition at an atomic scale, based on a realistic *n*-body Cu–Co potential, which was constructed with the aid of *ab initio* calculation.

(2) Molecular dynamics simulations predicted that an amorphous phase could be formed near the composition of $Cu_{60}Co_{40}$ and its atomic structure could be inhomogeneous, which was confirmed by the 200 keV Xe^+ ion beam mixing at low temperature.

(3) *Ab initio* calculations predicted that the metastable phase at the composition of $Cu_{75}Co_{25}$ could be of $L1_2$ (FCC) and $D0_{19}$ (HCP) structures, and that the metastable phase at the composition of $Cu_{25}Co_{75}$ could be of $D0_{19}$ (HCP) structure. In 200 keV Xe^+ ion beam mixing experiments performed at low temperature, the metastable phases obtained in the $Cu_{82}Co_{18}$ and $Cu_{26}Co_{74}$ samples, respectively, are quite compatible with the *ab initio* predicted ones near the respective compositions.

References

[1] Yavari A R, Desré P J and Benameur T 1992 *Phys. Rev. Lett.* **68** 2235
[2] Eckert J E, Holzer J C, Krill C E and Johnson W L 1993 *J. Appl. Phys.* **73** 2794
[3] Uenishi K, Kobayashi K F, Nasu S, Hatano H, Ishihara K N and Shingu P H 1992 *Z. Metallk.* **83** 132
[4] Liu B X, Johnson W L, Nicolet M A and Lau S S 1983 *Appl. Phys. Lett.* **42** 45
[5] Liu B X and Jin O 1997 *Phys. Status Solidi* a **161** 3
[6] Chien C L, Liou S H, Kofalt D, Yu W, Egami T and McGuire T R 1986 *Phys. Rev.* B **33** 3247
[7] Liu B X and Pan F 1993 *Phys. Rev.* B **48** 10276
[8] Krebs H U 1997 *Int. J. Non-Equilib. Process. (UK)* **10** 3
[9] Sumiyama K, Yoshitake Y and Nakamura Y 1985 *Acta Mater.* **33** 1785
[10] Liu B X, Lai W S and Zhang Q 2000 *Mater. Sci. Eng.* R **29** 1
[11] Thompson M W 1969 *Defects and Radiation Damage in Metals* (Cambridge: Cambridge University Press)
[12] De Boer F R, Boom R, Mattens W C M, Miedema A R and Niessen A K 1989 *Cohesion in Metals: Transition Metal Alloys* (Amsterdam: North-Holland)
[13] Zhang R F and Liu B X 2003 *J. Mater. Res.* **18** 7
[14] Bakker H 1998 *Enthalpies in Alloys: Miedema's Semi-Empirical Model* (Switzerland: Trans Tech)
[15] Alonso J A, Gallego L J and Simozar J A 1990 *Nuovo Cimento* **12** 587
[16] Zhang Q, Lai W S and Liu B X 1998 *Phys. Rev.* B **58** 14020
[17] Liu J B, Li Z C, Liu B X, Kresse G and Hafner J 2001 *Phys. Rev.* B **63** 132204
[18] Liu J B, Li Z F, Zhang J X, Liu B X, Kresse G and Hafner J 2001 *Phys. Rev.* B **64** 054102
[19] Lin C, Yang G W and Liu B X 2000 *Phys. Rev.* B **61** 15649
[20] Li Z F, Lai W S and Liu B X 2000 *Appl. Phys. Lett.* **77** 3920
[21] Servi I S and Turnbull D 1966 *Acta Metall.* **14** 161
[22] Da Silva F C S, Ferrari E F and Knobel M 1999 *J. Appl. Phys.* **86** 7170
[23] Krasnochtchekov P, Averback R S and Bellon P 2005 *Phys. Rev.* B **72** 174102
[24] Miranda M G M, Estévez-Rams E, Martínez G and Baibich M N 2003 *Phys. Rev.* B **68** 014434
[25] Meyer M and Pontikis V 1991 *Computer Simulation in Materials Science* (Dordrecht: Dordrecht Academic)
[26] Chadi D J 1979 *Phys. Rev.* B **19** 2074
[27] Weeber A W 1987 *J. Phys. F: Met. Phys.* **17** 809
[28] Niessen A K, Miedema A R, de Boer F R and Boom R 1988 *Physica* B **151** 401
[29] Kresse G and Hafner J 1993 *Phys. Rev.* B **47** 558
[30] Kresse G and Furthmüller J 1996 *Comput. Mater. Sci.* **6** 15
Kresse G and Furthmüller J 1996 *Phys. Rev.* B **54** 11169
[31] Vanderbilt D 1990 *Phys. Rev.* B **41** 7892
[32] Perdew J P and Wang Y 1993 *Phys. Rev.* B **45** 13244
[33] Monkhorst H J and Pack J D 1976 *Phys. Rev.* B **13** 5188
[34] Parrinello M and Rahman A 1981 *J. Appl. Phys.* **52** 7182
[35] Waseda Y 1980 *The Structure of Non-Crystalline Materials: Liquid and Amorphous Solids* (New York: McGraw-Hill)
[36] Ziegler J F, Biersack J P and Littmark U 1985 *The Stopping and Range of Ions in Solids* (New York: Pergamon)
[37] Haddad W S, Cullen D, Solem J C, Longworth J W, McPherson A, Boyer K and Rhodes C K 1992 *Appl. Opt.* **31** 24

[38] Ostwald W Z 1879 *Phys. Chem.* **22** 289
[39] Kittel C 1976 *Introduction to Solid State Physics* (New York: Wiley)
[40] Smith C J 1976 *Metal Reference Book* (London: Butterworths)
[41] Simmons G and Wang H 1971 *Single Crystal Elastic Constants and Calculated Aggregate Properties: a Handbook* (Cambridge, MA: MIT Press)
[42] Balluffi R W 1978 *J. Nucl. Mater.* **69/70** 240
[43] Cahn R W, Haasen P and Wollenberger H J 1983 *Physical Metallurgy* (Amsterdam: Elsevier)